Title
CALCIUM SULFATE-INDUCED CORROSION OF IRON-CHPOMIUM ALLOYS

Authors
Choi, S.H.
Stringer, J.

Publication Date
1985-08-01

LBL-20138
Preprint

Lawrence Berkeley Laboratory
UNIVERSITY OF CALIFORNIA

Materials & Molecular Research Division

Submitted to Corrosion Science

CALCIUM SULFATE-INDUCED CORROSION OF IRON-CHROMIUM ALLOYS

S.H. Choi and J. Stringer

August 1985

Prepared for the U.S. Department of Energy under Contract DE-AC03-76SF00098

DISCLAIMER

CALCIUM SULFATE-INDUCED CORROSION OF IRON-CHROMIUM ALLOYS

S.H.Choi* and J.Stringer†

* Materials and Molecular Research Division
Lawrence Berkeley Laboratory
University of California
Berkeley, CA 94720, U.S.A.

† Electric Power Research Institute
3412 Hillview Ave.
Palo Alto, CA 94304, U.S.A.

The calcium sulfate-induced corrosion behavior of binary Fe-Cr alloys has been studied at a temperature of 1223 K under an oxygen partial pressure of $10^{-11.2}$ atm, generated using a CO/CO_2 gas mixture. These conditions are intended to simulate the oxygen activities in the low oxygen partial pressure locations in the fluidized bed combustor. After exposure the surface and cross-section morphologies of the scale and alloy were examined using optical metallography and scanning electron microscopy. Qualitative chemical analysis of the scale was performed using an EDX unit attached to the SEM. Phase identification was carried out using X-ray diffraction. It was found that under this low oxygen activity, the presence of calcium sulfate induces sulfidation/oxidation corrosion. The formation of internal Cr-rich sulfide/oxide particles in the underlying alloy below an inner Cr-rich oxide layer was generally observed. The reaction products between the oxide and the calcium salts formed at the external surface of scale on iron-chromium alloys, such as a eutectic $CaO{\cdot}Cr_2O_3$ oxide mixture, appear to be insignificant in controlling the overall degradation process. The corrosion mechanism appears to be a sulfidation/oxidation process consistent with the low oxygen partial pressure and the relatively high sulfur activity calculated from the Ca-O-S equilibria.

1. Introduction

Sulfur is a critical impurity in almost all fossil fuel energy sources used in the power generation industries. In practical coal utilization situations structural alloys are exposed at high temperatures to atmospheres containing oxygen and sulfur. One example of a coal utilization industry in which sulfidation/oxidation corrosion is a potential problem, is fluidized bed combustion. This process, and its potential advantages, have been described in detail elsewhere[1]. The bed operating temperature is usually in the range of 1023-1223 K. Limestone may be added as a sulfur dioxide sorbent to bed to effectively reduce SO_2 emission release from the fuel during combustion. When this is done, calcium sulfate deposits on the hotter metal surfaces of the in-bed heat exchangers and the uncooled support structure. The oxygen partial pressure within the bed, measured using zirconia probes, fluctuates rapidly with minimum values which may be as low as 10^{-12} - 10^{-14} atm at a bed temperature of 1223 K[2,3]. The calcium sulfate deposited on the hotter metal surfaces could be decomposed locally in the local low oxygen partial pressure region, and consequently significant sulfur partial pressures would be developed[4,5].

It has been shown that sulfidation of some of the constituents of typical alloys is certainly possible[6]. The sulfur is present as sulfides in the metal ahead of the oxidation front: the presence of those sulfides appears to prevent the alloy forming a continuous protective Cr_2O_3 scale, and the alloy oxidizes rapidly. In many cases, the sulfides formed are chromium-rich, and it has been suggested that the rapid corrosion is due to the depletion of the chromium in the alloy. However, other studies have shown that the calcium itself may be a factor in the corrosion process[7,8,9]. The preformed Cr_2O_3 layer could be destroyed due to the formation of a compound oxide $CaO{\cdot}Cr_2O_3$ or $CaO{\cdot}Fe_2O_3$, which is capable of forming a low melting point eutectic.

Materials testing in a fluidized bed combustor is expensive and time consuming, and it is very difficult to determine the reaction mechanism. Thus, a simple laboratory method which may give comparable results is valuable. A simple laboratory crucible experiment to determine the reaction mechanism was performed by Stringer and Whittle[5], studying commercial alloys such as Incoloy 671 and Type 316 stainless steel, in a $CaSO_4$/graphite powder mixture in a crucible. The role of the graphite, it was suggested, was to keep the oxygen partial pressure low enough to decompose the $CaSO_4$. It was demonstrated that sulfidation/oxidation attack of alloys similar to that observed in actual combustors can be induced in calcium sulfate at low enough oxygen activities. Mark, Lin, Stevenson and Stringer[10] extended this study, using environments of $CaSO_4$/CaO powder mixtures and CO/CO_2 gas mixtures having a range of oxygen partial pressures, and exposing commercial alloys such as Type 304 stainless steel and Incoloy 800. They showed that sulfidation/oxidation type attack of the alloys, especially preferential penetration of sulfides along the grain boudaries of the alloy, is responsible for the rapid corrosion. Akuezue[9] demonstrated that the formation of a $CaO{\cdot}Fe_2O_3$ compound with a spinel structure appeared to be associated with the rapid corrosion of alloys. Various mixtures of $CaSO_4$, CaO and graphite powders, and several materials such as pure Fe, Fe-Cr alloys, stainless steel, Incoloy etc were used in this laboratory study.

In the present study, the corrosion type and the attack mode induced by calcium sulfate on the protective Cr_2O_3 scale and the alloy were examined in environments of controlled oxygen and sulfur partial pressures connected through the $CaSO_4$/CaO/CaS equilibria, using $CaSO_4$/CaO powder mixture in a crucible and CO/CO_2 gas mixtures to define the oxygen partial pressure. Ferritic binary Fe-Cr alloys were chosen as the Cr_2O_3-formers in part because alloys of this type are candidates for in-bed components, and in part to avoid the complication of the presence of nickel in the austeni-

tic stainless steel alloys. Iron and chromium are the major components present in the stainless steels used in applications such as coal combustion. The morphological changes in the scale and the scale-alloy interface, the phase distribution in the reaction product, and the development of corrosion have been observed, to obtain further metallographic evidence to establish the reaction characteristics more fully. Emphasis was placed on the distribution of sulfide in the alloy which usually determines the overall rate of material degradation.

2. Experimental

2.1. Specimen preparation

The iron-chromium alloys were melted in an induction furnace under vacuum, and cast into 50 mm diameter ingots. The chemical compositions of the alloy ingots are shown in Table 1. The cast ingots were homogenized at 1473 K for 24 hours. The alloys were then cut into test coupons measuring approximately 10 x 10 x 1 mm. The specimens were wet polished on SiC papers ranging from 180 grit to 600 grit under flowing water, and then thoroughly washed with soap solution, distilled water and ethanol. Prior to oxidation the dimensions of each test sample were measured using a micrometer. To determine the amount of oxidation which had occurred, the weight of each specimen was measured using an analytical torsion balance before and after each oxidation test.

2.2. Corrosion experiments.

The oxidation tests were conducted in a vertical tube furnace at a temperature of 1223 K for different time intervals up to 200 hours. The specimens were wholly immersed in the powder bed. The detailed experimental conditions are shown in Table 2. Mixtures of reagent grade $CaSO_4$ and CaO were used. A gas mixture of CO-CO_2 having a specified oxygen activity was passed over the powder bed. The certified grade CO-CO_2 gas mixtures were supplied premixed by Matheson Gas

Products Co. The oxygen partial pressure of $10^{-11.2}$ atm was selected based on the measured values of CO-content in the gas in a fluidized bed using a zirconia probe. The local P_{O_2} and P_{S_2} near the specimens inside the powder bed were calculated from the CO-CO_2 equilibria and the $CaSO_4$-CaO equilibria. Figure 1 shows the schematic diagram of the experimental apparatus. The alumina crucible containing the specimens immersed completely in the powder mixture was introduced from the top of the furnace, supported by an alumina rod attached to the crucible with alumina pins. After purging the apparatus with dry argon gas, the premixed gas mixture was admitted to the reaction chamber, and then the crucible was lowered to the furnace hot zone. At the completion of an oxidation run, the specimens were raised to the cold part while flushing with argon.

2.3. Analysis of corrosion products

After oxidation, the bed material adhering to the external surface of the oxidized specimens was removed, by blasting off dust with compressed air and then by ultrasonic cleaning with ethanol solution. After weighing, each test specimen was cold-mounted in epoxy resin and sectioned for metallographic examination. The mounted specimens were wet ground mechanically in cross-section using SiC abrasive papers from 180 grit to 600 grit, and then ground finely on alumina papers using lapping oil. Fine details of the cross-section were resolved after fine polishing by using 1 μm diamond paste under flowing Kerosene oil. The unetched cross-section morphologies of the scale and alloy were first examined using optical metallography. Following this examination of the unetched specimen, Villela's reagent(5 ml HCl, 1 g picric acid, 100 ml ethanol) was used as an etchant to reveal the grain boundaries of the alloy. Alternatively, a 10% bromine-90% methanol solution was used to dissolve away the metal, revealing the morphology of the inner surface of scale at the scale-alloy interface without destroying the scale mechanically, irrespective of whether the scale was in

direct contact with alloy or separated from it. The morphology of the scale and alloy in cross-section after etching by Villela's reagent or by the bromine-methanol solution were examined in the optical microscope and then in more detail using the Scanning Electron Microscope(SEM). In the latter case, the specimens were coated with conducting materials. Carbon was used mainly for coating the specimen surface, and sometimes aluminum and gold were also used. The morphologies of the outer surface, of the fractured section and of the inner surface of the stripped scale were also observed carefully using the SEM.

The chemical analysis of the corrosion products was carried out with an Energy Dispersive Analysis of X-rays(EDX) unit attached to the SEM. The elements present were identified from the peak positions and analyzed quantitatively from the net intensity after substracting the background. The spatial distribution of each element was determined mainly from the EDX elemental mapping of selected areas, and less frequently from line-scans, as well as from quantitative analysis of small selected areas.

The major crystallographic phases present in the corrosion products were identified using X-ray diffraction(XRD). A X-ray diffractometer using Cu-K_α radiation and Ni-filter step-scanned at a very slow speed of the order of 1°/min, on the external surface of oxidized samples and less frequently on the outer surface of the descaled alloy substrate. The phases present in the scale were identified from the characteristic peak positions and the corresponding intensities.

3. Results

3.1. Kinetics

Figure 2 shows the weight gain of the Fe-20Cr alloy and the Fe-25Cr alloy as a function of exposure time in the low external P_{O_2} environment($P_{O_2}=10^{-11.2}$ atm) in the $CaSO_4/CaO$ mixture at 1223 K, illustrating the effect of the Cr-content in the alloy. At the early stage of oxidation until 100 hours, the Fe-20Cr alloy showed better

oxidation resistance than the Fe-25Cr alloy. The weight change of the Fe-20Cr and the Fe-25Cr alloy after 100 hours oxidation was 2.07 mg/cm^2 and 3.10 mg/cm^2, respectively. Breakaway kinetics was observed after an exposure of 150 hours in the Fe-20Cr alloy. In the Fe-25Cr alloy, the weight change increased slightly as the reaction time increased, still showing protective behavior.

3.2. Scale morphology and chemical composition.

As the chromium content in the alloy was increased, the scale formed on the alloy surface became thin, and the chromium content in the scale was increased. A thin adherent Cr_2O_3 scale was formed nearly uniformly on the alloy surface at the early stage of oxidation, from the 20 wt.% Cr in the alloy. Even in the $CaSO_4$-containing environments, no internal sulfidation was observed in the Fe-25Cr alloy. However, the Fe-20Cr alloy oxidized severely showing the characteristics of sulfidation, and the Fe-18Cr alloy oxidized more rapidly also showing sulfidation. The following discussion refers mainly to the Fe-20Cr alloy.

Figure 3 illustrates the breakaway process for the Fe-20Cr alloy in the $CaSO_4/CaO$ mixture in the low external P_{O_2} environment($P_{O_2}=10^{-11.2}$ atm) at 1223 K. Cross-section morphologies consistent with the kinetic curve shown in Figure 2 exhibit the breakaway process of the thin compact chromium oxide scale to a thick two-layer scale composed of an outer Fe-oxide layer and an inner mixed Fe-Cr oxide layer. The protective chromium oxide scale formed on the Fe-20Cr alloy had broken away after 150 hours oxidation. Figure 3a, 3b, 3c, and 3d show the compact chromium-rich oxide scale with a thickness of about 3-4 μm, 6 μm, 9-10 μm, and 14-15 μm, respectively. The scale had grown gradually as the exposure time increased. At the early stage of oxidation, the grain size of oxide was about 1 μm in the thin adherent chromium oxide scale with a thickness of about 5 μm. The morphology of the scale at the scale-alloy interface was wavy. Figure 3e shows the two-layered scale, with a thickness of 50 μm,

which was composed of an outer iron-rich oxide layer and an inner Cr-rich oxide layer. After the thickening and the separation of the scale, the overall scale was composed of two layers; an outer thick iron-rich oxide layer, and an inner relatively thin Cr-rich oxide layer. The external scale contained little or no chromium, no sulfur, and apparently no calcium at least close to the interface. The inner chromium-rich oxide layer contained some iron-rich regions which appeared under the optical microscope to be metallic iron. Figure 3f shows the thick two-layered scale composed of an outer Fe-rich oxide layer and an inner mixed Fe-Cr oxide layer, which gradually spreads, destroying the remaining protective scale; part of the scale is still protected by the chromium oxide, part shows the thick scale. The inner mixed Fe-Cr oxide layer was more porous and non-compact. The innermost thin chromium-rich oxide layer with a thickness of approximately 5-10 μm was formed near the scale-alloy interface.

In the metal, isolated particles rich in Cr and S but very low in Fe were detected. The maximum depth of the internal sulfidation zone containing Cr-rich sulfide particles below the inner chromium oxide layer was approximately 20-30 μm in the Fe-20Cr alloy. It is possible that oxides or oxysulfides might have been present in this zone, but in the absence of an oxygen-distribution determination it is not possible to be sure. However, the appearance of all the particles is consistent with their being CrS. Discrete internal chromium-rich sulfide particles were globular in shape and aligned to a constant depth in the alloy parallel to the scale-alloy interface. Oxide intrusion into the alloy matrix, containing some sulfur, and globular Cr-rich sulfide particles just below them were also observed. Figure 4 shows an SEM micrograph exhibiting the cross-section morphology of an Fe-20Cr alloy oxidized for 150 hours in the $CaSO_4/CaO$ mixture in the low external P_{O_2} environment($P_{O_2}=10^{-11.2}$ atm) at 1223 K. Figure 5 shows the sulfur distribution through the thick two-layer scale. Sulfur was detected at the boundary region between an outer Fe-rich oxide and an inner Cr-rich

oxide, and between an inner Cr-rich oxide and alloy. Sulfur was also randomly distributed in the Cr-rich region in the scale. The observation of Cr-rich sulfides within and just below the thick two-layer scale suggests that this internal attack may be correlated with the formation and growth of the thick scale. There was a strong tendency for the scale to spall off more easily in the sulfur-containing environment, indicating that sulfur may be closely related with the non-adherency and the premature breakaway of the Cr_2O_3 scale.

A scale composed of an outer (Ca/Cr) oxide layer and an inner Cr-rich oxide layer was produced on the Fe-20Cr alloy surface locally, as shown in Figure 6. The (Ca/Cr) oxide formed on the external surface of the oxidized samples as a reaction product appears to be a mixture of CaO and Cr_2O_3, based on the EDX analysis results and on the CaO-Cr_2O_3 phase diagram. In all cases, the mixture of CaO and Cr_2O_3 was uniformly distributed, not too thick, and did not reach the bare alloy surface, which was always well covered by the inner Cr-rich oxide layer. The CaO and Cr_2O_3 oxide mixture was also formed on the external surface of the oxidized samples as a reaction product, with the iron oxide just above the thin Cr-rich oxide layer. The CaO and Fe_2O_3 oxide mixture was not continuously distributed, and not deep enough to penetrate through the thin Cr-rich oxide layer, reaching the scale-alloy interface. No Ca-bearing species were detected at or below the scale-alloy interface. $CaO{\cdot}Cr_2O_3$ or $CaO{\cdot}Fe_2O_3$ single phase was not detected on the surface of the oxidized samples by XRD in any case, just a mixture was observed in the microscope. There was no evidence of compound oxide formation, either in the Ca-Fe-O or Ca-Cr-O system.

4. Discussion

Calcium sulfate is solid and thermodynamically stable in air in the temperature range 1023-1223 K[11]; this is the operating temperature range of a fluidized bed combustor. However, calcium sulfate deposited on the hotter metal surfaces in

fluidized bed combustors would be decomposed to SO_2 at a relatively low oxygen partial pressure.

$$CaSO_4 = CaO + SO_2 + 1/2\ O_2$$

$$SO_2 = 1/2\ S_2 + O_2$$

Figure 7 shows the thermodynamic phase stability diagram for the Ca-O-S system at 1223 K[12]. If the oxygen partial pressure is sufficiently low, the sulfur activity could be increased theoretically to a level equal to that at the $CaSO_4/CaO/CaS$ triple point within the bed of a fluidized bed combustor. In other words, the sulfur activity within the bed could be increased to $10^{-3.5}$ atm at 1223 K.

The severe sulfidation/oxidation type attack induced by $CaSO_4$ occurred locally, as shown in Figure 8, accompanying the breakaway of the protective chromium oxide scale on the iron-chromium alloy. It is believed that the sulfur activity is increased high enough to sulfidize the alloy along the $CaSO_4/CaO$ equilibrium line as a direct consequence of the low oxygen partial pressure. This indicates that generation of a sulfidizing gas mixture by the principal components of a compact deposit, i.e. $CaSO_4$ and CaO, is a possible mechanism of sulfidation relevant to fluidized bed combustor. In other words, the sulfur-containing species was evolved from the $CaSO_4/CaO$ equilibrium in the low oxygen partial pressure atmospheres created by the CO/CO_2 gas mixture.

Iron-rich oxides, chromium-rich sulfides and Cr_2O_3 developed as corrosion products. A solid state reaction between a $CaSO_4$ deposit and a protective Cr_2O_3 scale is probable, but not serious. The reaction products formed at the external surface of the scale on the iron-chromium alloys, such as a CaO and Cr_2O_3 oxide mixture and a CaO and Fe_2O_3 oxide mixture appear to be insignificant in controlling the overall corrosion mechanism. In the environment of a moderately low oxygen partial pressure and a relatively high sulfur partial pressure, Cr-rich sulfides were formed below and within

the scale. The chromium content in the alloy was critical i.e. low chromium alloys such as Fe-15Cr and Fe-18Cr were more susceptible to sulfidation/oxidation type attack. A uniform band of discrete globular chromium sulfide particles below an inner thin chromium-rich oxide layer was the most common observation locally, which seems to be significant in the long-term oxidation.

The distribution of the internal Cr-rich sulfide particles in the alloy seems to be critical, as well as the chromium depletion caused by the sulfur pick-up locally. Internal sulfidation of the metal below an inner thin chromium oxide could be a precursor to breakaway corrosion.

5. Conclusion

Calcium sulfate coupled with local low oxygen activities induces sulfidation/oxidation corrosion. The general appearance of the corrosion microstructure is consistent with the sulfur activity expected from a consideration of the Ca-O-S stability diagram. Reaction between the protective oxide and the calcium containing salts may occur, but does not appear to play a significant role in the corrosion process.

6. Acknowledgements

This work was supported by the Director, Office of Energy Research, Office of Basic Energy Sciences, Materials Sciences Division of the U. S. Department of Energy under Contract Number DE-AC03-76SF00098.

References

1. J.Stringer, "High temperature corrosion problems in the electric power industry and their solution." ed Robert A. Rapp, Sandiego, 1981
2. M.J.Cooke, A.J.B.Cuttler and E.Raask, J.Inst.Fuel, 45(1972)153
3. A.J.Minchener et al, EPRI Final report CS-1853 Research Project 979-1, May, 1981
4. J.Stringer and S.Ehrlich, "High temperature corrosion in fluidized bed combustors." ASME Annual Meeting, December, 1976, paper no 76-WAS/CD-4
5. J.Stringer and D.P.Whittle, Proc. Int. VDG Conf. on Corrosion and Deposition in Power plants, Essen, June, 1977
6. J.Stringer, "High temperature corrosion in fluidized bed combustion." Ash Deposits and Corrosion due to Impurities in Combustion Gases, ed R.W.Bryers, Hemisphere, Washington,D.C. 1977
7. S.R.J.Saunders, M.K.Hossain, B.Kent and D.M.Loyd, High temperature technology, 2(1984)63-73
8. R.A.Perkins, Personal communication
9. H.Akuezue, M.S.Thesis, LBL, University of California, Dec. 1979
10. J.Stringer, K.Mark and J.S.Lin, Proc. Electrochem. Soc. Sym. on High Temperature Materials (1983) San Francisco
11. H.H.Kellogg, Trans. Met. Soc. AIME, 230(1964)1622
12. I.Barin, O.Knacke and O.Kubaschewski, "Thermochemical properties of Inorganic substances." Springer-Verlag, New York, 1973, 1977

Figure captions

Figure 1. Schematic diagram of experimental apparatus.

Figure 2. The variation of weight gain of Fe-20Cr and Fe-25Cr as a function of exposure time.

Figure 3. Optical cross-section morphology of Fe-20Cr oxidized in the $CaSO_4/CaO$ mixture in the low external P_{O_2} environment ($P_{O_2}=10^{-11.2}$ atm) at 1223 K.

Figure 4. Scanning micrograph showing the cross-section morphology of Fe-20Cr oxidized for 150 hours in the $CaSO_4/CaO$ mixture in the low external P_{O_2} environment at 1223 K.

Figure 5. Scanning micrograph showing the cross-section morphology of Fe-20Cr oxidized in the $CaSO_4/CaO$ mixture in the low external P_{O_2} environment ($P_{O_2}=10^{-11.2}$ atm) for 200 hours at 1223 K.

Figure 6. Scanning micrograph showing the cross-section morphology of Fe-20Cr oxidized in the $CaSO_4/CaO$ mixture in the low external P_{O_2} environment ($P_{O_2}=10^{-11.2}$ atm) for 200 hours at 1223 K. Fe-, Cr-, Ca- and S-line scan through the scale.

Figure 7. Simplified stability diagram for the Ca-O-S system, Fe-O-S system, and Cr-O-S system at 1223 K.

Figure 8. A schematic of the corrosion induced in Fe-Cr alloys in the presence of $CaSO_4$ and a low oxygen partial pressure atmosphere.

Table 1. Chemical composition of alloys tested.
(unit : weight percentage)*

nominal composition	Fe	Cr
Fe-15Cr	84.40	15.60
Fe-18Cr	81.82	18.18
Fe-20Cr	79.24	20.76
Fe-25Cr	74.22	25.78
Fe-30Cr	69.63	30.37

* analyzed in EDX

Table 2. Experimental conditions in crucible test.

alloy tested	:	Fe-15Cr, Fe-20Cr, Fe-25Cr
temperature	:	1223 K
external environment	:	1.2% CO - 98.8% CO_2 , $P_{O_2} = 10^{-11.2}$ atm
gas flow rate	:	0.1 cm/sec
powder bed	:	$CaSO_4/CaO$ (38mm diameter x 38mm height)
environment inside bed* (near specimen surface)	:	$P_{O_2} = 10^{-11.2}$, $P_{S_2} = 10^{-4.5}$ atm
duration	:	25, 50, 100, 150, 200 hours

* thermodynamically calculated value.

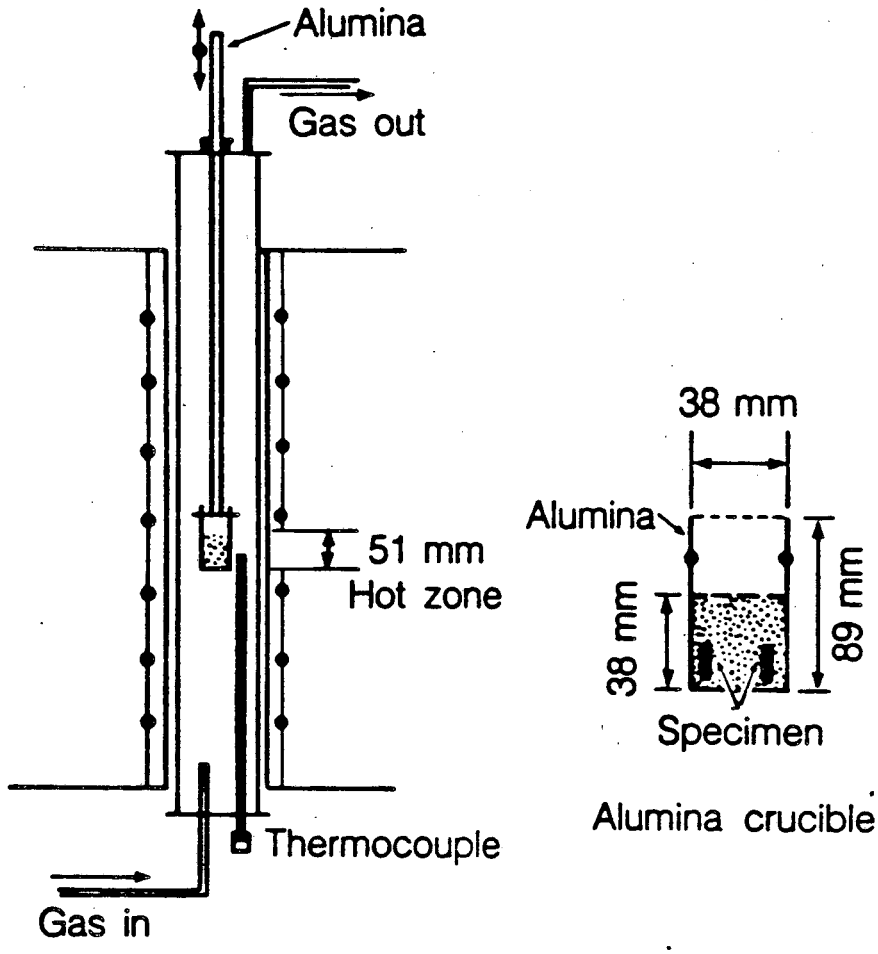
Alumina
Gas out
51 mm
Hot zone
Thermocouple
Gas in
38 mm
Alumina
38 mm
89 mm
Specimen
Alumina crucible
XBL 856-10023

Figure 1.

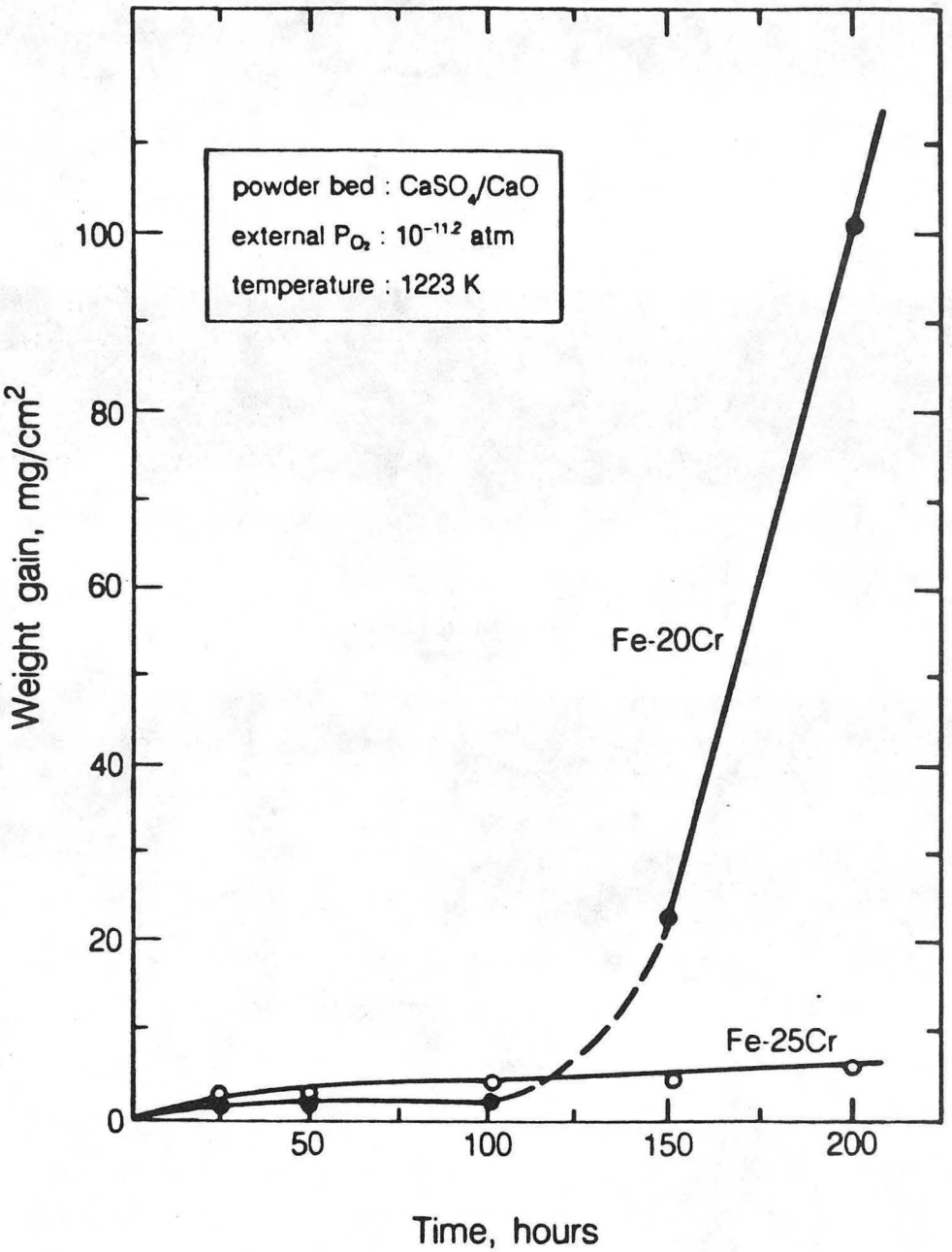
powder bed : $CaSO_4/CaO$
external P_{O_2} : $10^{-11.2}$ atm
temperature : 1223 K
Weight gain, mg/cm^2
0
20
40
60
80
100
50
100
150
200
Time, hours
Fe-20Cr
Fe-25Cr
XBL 856-10021

Figure 2.

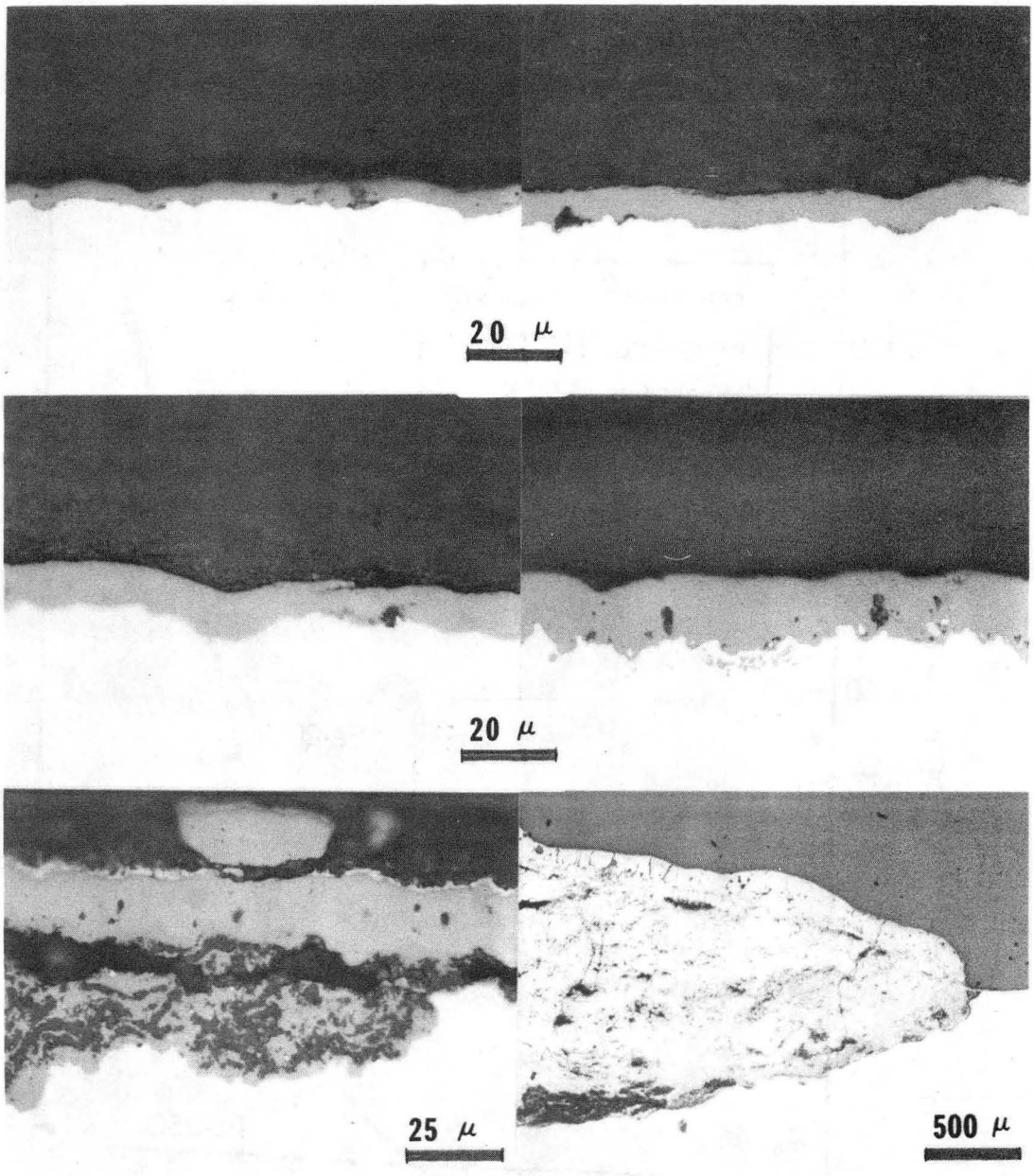

XBB 838-7057

Figure 3.

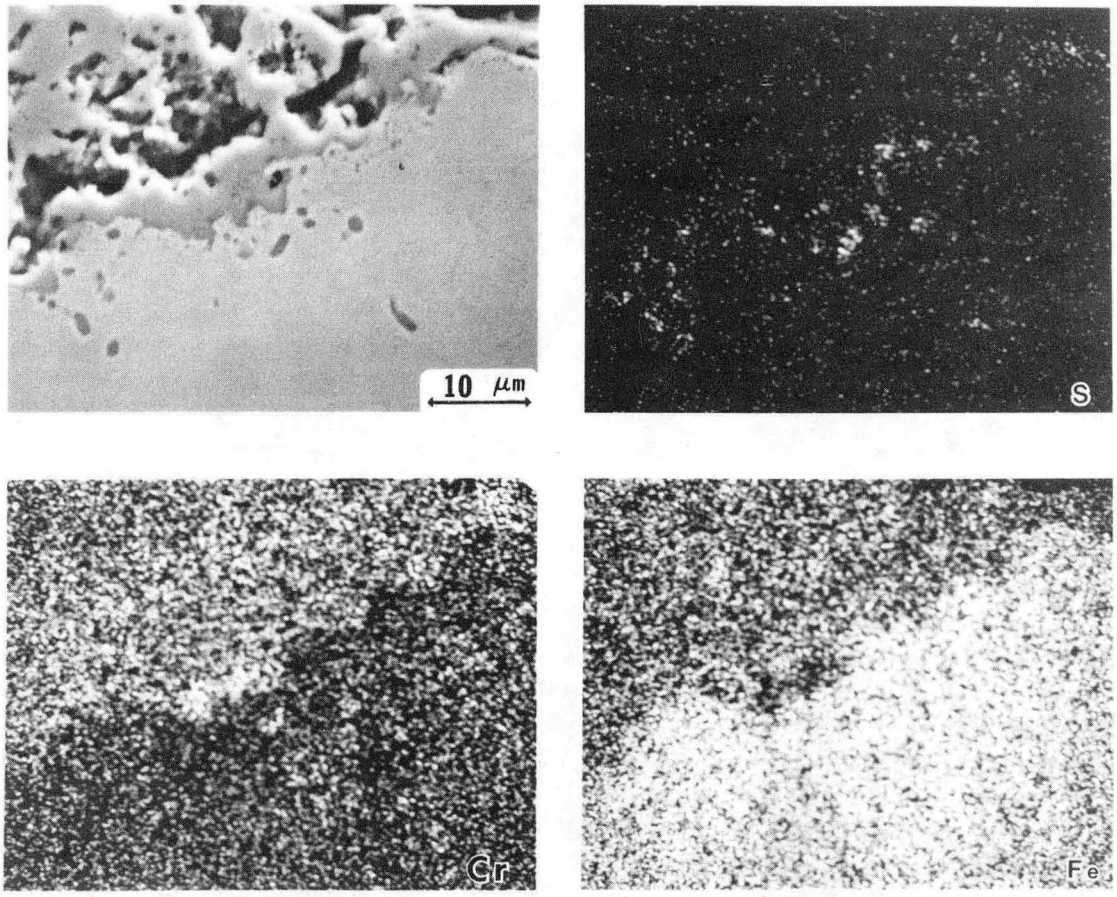

XBB 856-4556

Figure 4.

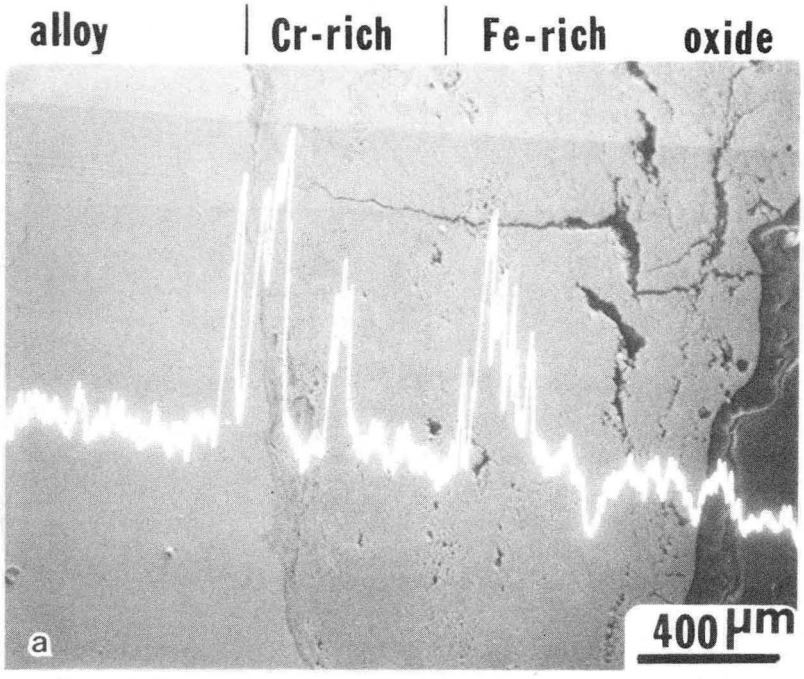

S-line

S-map

XBB 856-4577

Figure 5.

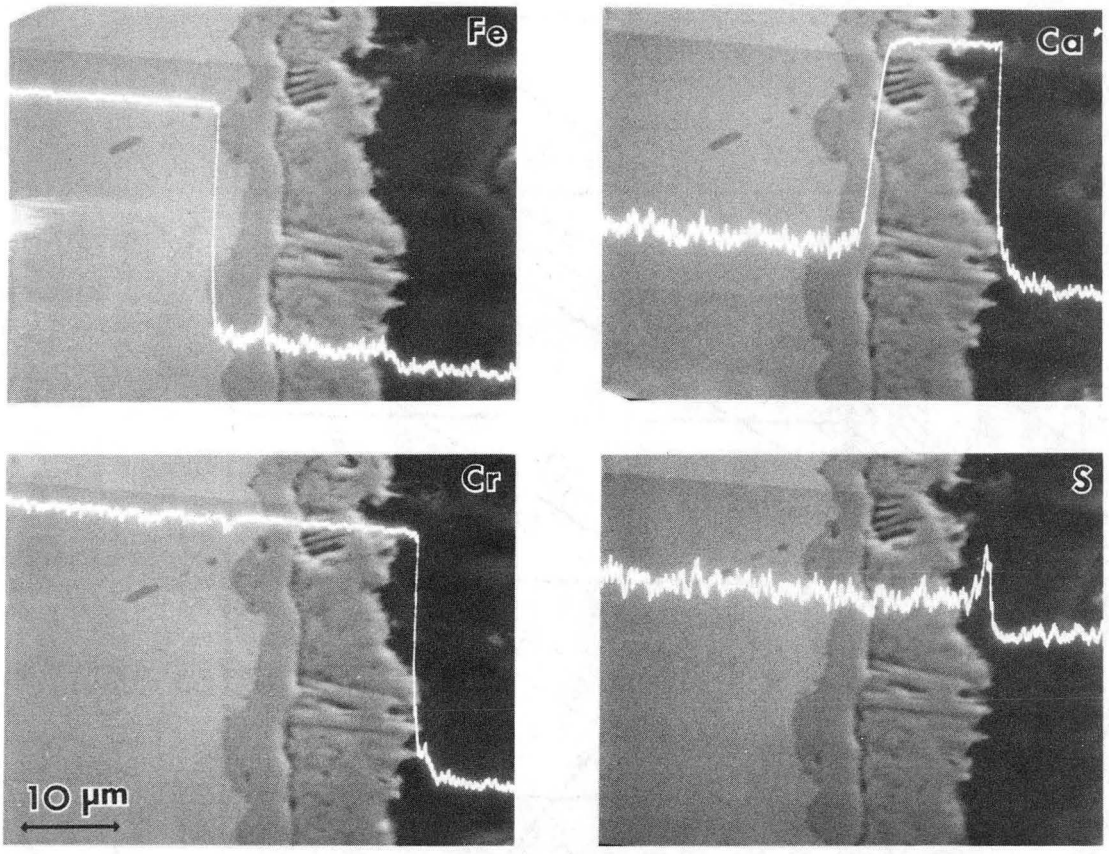

XBB 856-4577

Figure 6.

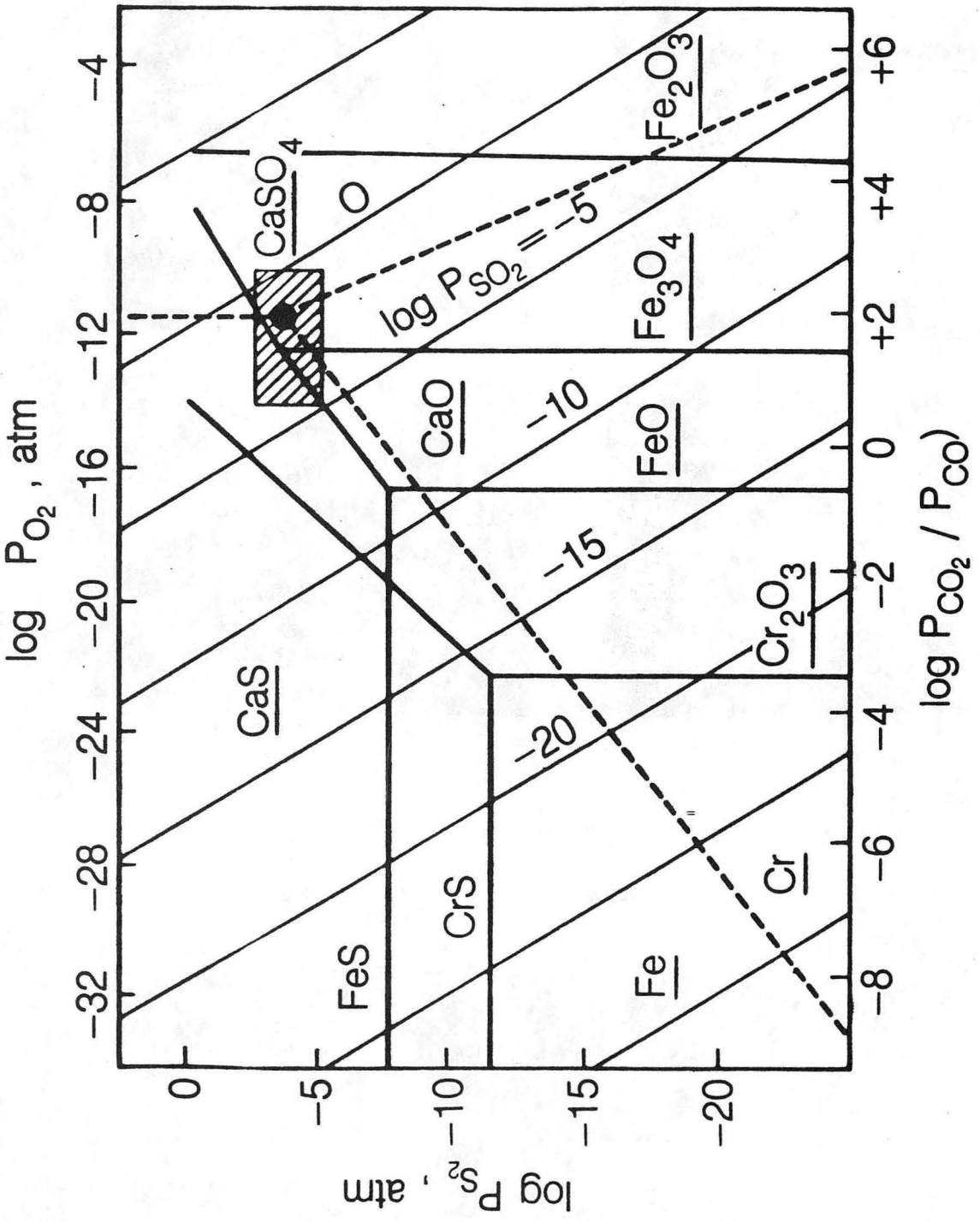
log P_{O_2}, atm
log P_{S_2}, atm
log P_{CO_2} / P_{CO})
$CaSO_4$
O
Fe_2O_3
log P_{SO_2} = −5
Fe_3O_4
CaO
−10
FeO
−15
Cr_2O_3
−20
CaS
FeS
CrS
Fe
Cr

Figure 7.

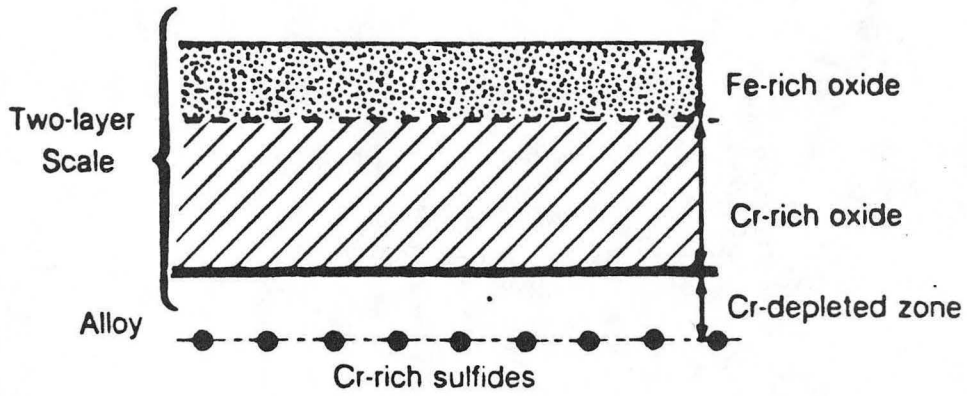
Two-layer
Scale
Fe-rich oxide
Cr-rich oxide
Cr-depleted zone
Alloy
Cr-rich sulfides
XBL 856-10018

Figure 8.

LAWRENCE BERKELEY LABORATORY
TECHNICAL INFORMATION DEPARTMENT
UNIVERSITY OF CALIFORNIA
BERKELEY, CALIFORNIA 94720